Geophysical Research Letters

RESEARCH LETTER
10.1029/2019GL084150

Key Points:
- Dust impact signals detected by Cassini can be understood as spacecraft potential perturbation due to the impact-generated charges
- The shape of impact signal is consistent with the separate movements ofthe electrons and ions of the impact plasma
- Better-controlled laboratory simulations of Cassini observations improved the understanding of impact signal generation

Supporting Information:
- Supporting Information S1

Correspondence to:
S.-Y. Ye,
yesy@sustech.edu.cn

Citation:
Ye, S.-Y., Vaverka, J., Nouzak, L., Sternovsky, Z., Zaslavsky, A., Pavlu, J., et al. (2019). Understanding Cassini RPWS antenna signals triggered by dust impacts. *Geophysical Research Letters*, *46*. https://doi.org/10.1029/2019GL084150

Received 17 JUN 2019
Accepted 30 AUG 2019
Accepted article online 4 SEP 2019

Understanding Cassini RPWS Antenna Signals Triggered by Dust Impacts

S.-Y. Ye[1,2], J. Vaverka[3], L. Nouzak[3], Z. Sternovsky[4], A. Zaslavsky[5], J. Pavlu[3], I. Mann[6], H.-W. Hsu[4], T. F. Averkamp[2], A. H. Sulaiman[2], D. Pisa[7], G. B. Hospodarsky[2], W. S. Kurth[2], and M. Horanyi[4]

[1]Department of Earth and Space Sciences, Southern University of Science and Technology (SUSTech), Shenzhen, China, [2]Department of Physics and Astronomy, The University of Iowa, Iowa City, IA, USA, [3]Faculty of Mathematics and Physics, Charles University, Prague, Czechia, [4]LASP, University of Colorado Boulder, Boulder, CO, USA, [5]Observatoire de Paris, Meudon, France, [6]Department of Physics and Technology, The Arctic University of Norway, Tromso, Norway, [7]Department of Space Physics, IAP CAS, Prague, Czechia

Abstract Electric field antennas are capable of detecting dust impacts in different space environment. We analyze the dust impact signals detected by the Cassini Radio and Plasma Wave Science instrument at different locations around Saturn and compare them with dust impact signals simulated in laboratory conditions and numerically. The spacecraft potential, the size, and capacitance of the impacted element and ambient plasma have a strong effect on the amplitude and the shape of impact signals, providing important clues to understanding the signal generation mechanism. The voltage signal on the antenna is due to the separation of the impact generated charges, which occurs as electrons and ions can either escape (at different speeds) or be collected by the impacted element depending on the spacecraft potential.

1. Introduction

Electric field antennas onboard spacecraft have been used to detect dust impacts in space for several decades (Aubier et al., 1983; Gurnett et al., 1983; Gurnett et al., 1987; Gurnett et al., 1991; Kelley et al., 2012; Kurth et al., 2006; Meyer-Vernet et al., 1996; Meyer-Vernet et al., 2009; Pedersen et al., 1991; Tsintikidis et al., 1994; Tsintikidis et al., 1995; Wang et al., 2006). However, the generation mechanism of the voltage pulses has not been well understood. A number of models have been proposed to interpret the signals observed (Meyer-Vernet et al., 2017; Oberc, 1996; Zaslavsky, 2015), but the variability of the signals observed by different spacecraft at different locations sometimes makes the interpretation difficult (Kellogg et al., 2016, 2018; Malaspina et al., 2014, 2015; Malaspina & Wilson, 2016; O'Shea et al., 2017; Tsurutani et al., 2004; Vaverka et al., 2017a; Zaslavsky et al., 2012).

The Cassini Radio and Plasma Wave Science (RPWS) instrument (Gurnett et al., 2004) detected dust impact signals in different regions of Saturn's magnetosphere (Ye et al., 2014; Ye, Gurnett, et al., 2016; Ye, Kurth, Hospodarsky, Persoon, Gurnett, et al., 2018; Ye, Kurth, Hospodarsky, Persoon, Sulaiman, et al., 2018). The variations in the shapes of these signals reflect the changes in plasma conditions in these regions, spacecraft potential, instrument operating mode, and impact location. In this study, we analyze the dust impact waveforms detected in space by Cassini and in recent laboratory simulations and compare them to numerical simulations, which results in a consistent and relatively simple physical picture of the signal generation process.

2. Impact Ionization and Plasma Cloud Expansion

When a dust particle impacts a spacecraft at velocity higher than about 1 km/s, ~20–40% of the kinetic energy is converted to thermal energy vaporizing the impactor and part of the surface material (Braslau, 1970), which upon ionization generates a plasma cloud expanding rapidly away from the surface. The expansion of the impact plasma cloud can be roughly divided into three stages (Pantellini, Landi, et al., 2012; Tarantino et al., 2018). In the first stage, the plasma is a nonideal, collisional expanding plasma, because the mean free path of the electrons l_e is significantly shorter than the size of the cloud R_c (product of expansion speed and time). In the second stage (collisionless quasi-neutral expansion), $l_e \gg R_c$ and the charged

particles in the plasma cloud are still interacting with each other. In the third stage, the Debye length λ_D is much larger than the cloud size R_c; the plasma enters the single particle motion regime, so the particles can freely expand away from the impact site. Spacecraft potential relative to the ambient plasma can suppress or enhance the escape of particles, depending on the polarities (Hew et al., 2018). Electrons escape faster than ions, creating two fronts of escaping charges. The ambipolar electric field between the two species induces oscillation in the quasi-neutral plasma, generating electromagnetic pulses hazardous to the spacecraft electrical system (Close et al., 2013). The first two stages of the expansion are extremely fast, and the time scale (can be as short as nanoseconds) varies greatly with impact speed (Fletcher et al., 2015; Lee et al., 2013). So the voltage signals (the rising part usually lasts tens of microseconds) detected by the electric antennas are induced by the charge separation in the third stage of the expansion (Meyer-Vernet et al., 1986).

Simulation of plasma production due to hypervelocity impact has been carried out in multiple studies (Li et al., 2014; Fletcher et al., 2015; Song et al., 2015, 2016). Experimental measurements showed that the amount of charges generated by the dust impact scales strongly with impact velocity and also depends on particle mass and target material (Collette et al., 2014; Grün, 1984; McBride & McDonnell, 1999; Ratcliff et al., 1997). Significant differences exist between the findings of these studies, suggesting that other factors (e.g., surface cleanliness) may also play a role. The steep dependence on impact velocity makes this method sensitive to impacts by nanometer sized particles in the solar wind, which are accelerated by the solar magnetic field to hundreds of kilometers per second (Schippers et al., 2014, 2015).

3. Cassini RPWS Measurements

A detailed description of the RPWS instrument can be found in Gurnett et al. (2004). The three electric field antennas (E_U, E_V, E_W) are each 10 m long and 2.86 cm in diameter. The RPWS Wideband receiver (WBR) can be configured to measure either the potential difference between the E_U and E_V antenna (E_X dipole mode) or that between E_W and the spacecraft (E_W monopole mode). It has been known that a monopole antenna is more sensitive to dust impacts than a dipole antenna (Meyer-Vernet, 1985; Meyer-Vernet et al., 2014; Ye et al., 2014). Both Cassini observations and laboratory simulations showed evidence that the monopole mode is primarily sensitive to impacts on the spacecraft body and the E_W antenna whereas the dipole mode is primarily sensitive to impacts on the E_U and E_V antennas (Nouzak et al., 2018; Ye, Kurth, Hospodarsky, Averkamp, & Gurnett, 2016). Therefore, the effective impact area for the monopole mode is much larger than that of the dipole mode. Ye et al. (2014) pointed out that the polarity of the signals observed in the monopole mode depends on the spacecraft potential.

During Cassini's first Grand Finale orbit, the region between Saturn and its rings was found to be devoid of micron dust grains (Hsu et al., 2018; Mitchell et al., 2018). Four of the few micron dust impacts detected by RPWS were compared by Ye, Kurth, Hospodarsky, Persoon, Sulaiman, et al. (2018), which showed that the decay time scale of the impact signal decreases with increasing plasma density. Inside the ionosphere of Saturn, where the plasma density was on the order 1,000/cc (Wahlund et al., 2018), the decay time became comparable to the rise time, making it hard to differentiate dust impacts from solitary waves (Pickett et al., 2015; Vaverka et al., 2018).

Raw waveforms of the dust impact signals detected by RPWS WBR (monopole mode) at various locations in Saturn's magnetosphere (Figure 1) show that the rise and decay time scales tend to be longer in regions of lower plasma density, for example, at larger radial distances and higher latitudes (Ye, Kurth, Hospodarsky, Persoon, Sulaiman, et al., 2018). The polarities of the signals detected in the monopole mode are mostly positive (for impacts on spacecraft body) outside 10 R_S, where the spacecraft was charged positively (Ye et al., 2014). This is consistent with the observation in the E ring where the spacecraft potential was negative and most of the impact signals detected in the monopole mode were negative.

One feature rarely observed in space is the smaller and faster voltage pulse right before the main pulse, which is often referred to as “pre-spike” (Figures 1f, 1g, 1i, and 1j). These pre-spikes seem to be detected in regions of Saturn's magnetosphere where the spacecraft potential was close to zero (around 7 R_S and during the Grand Finale orbits). Note that the time scale of the pre-spike is comparable to the time between two adjacent samples, so it is possible that these features occur more often than they are observed by the instrument. The pre-spikes have also been observed by Solar TErrestrial RElations Observatory and Magnetospheric

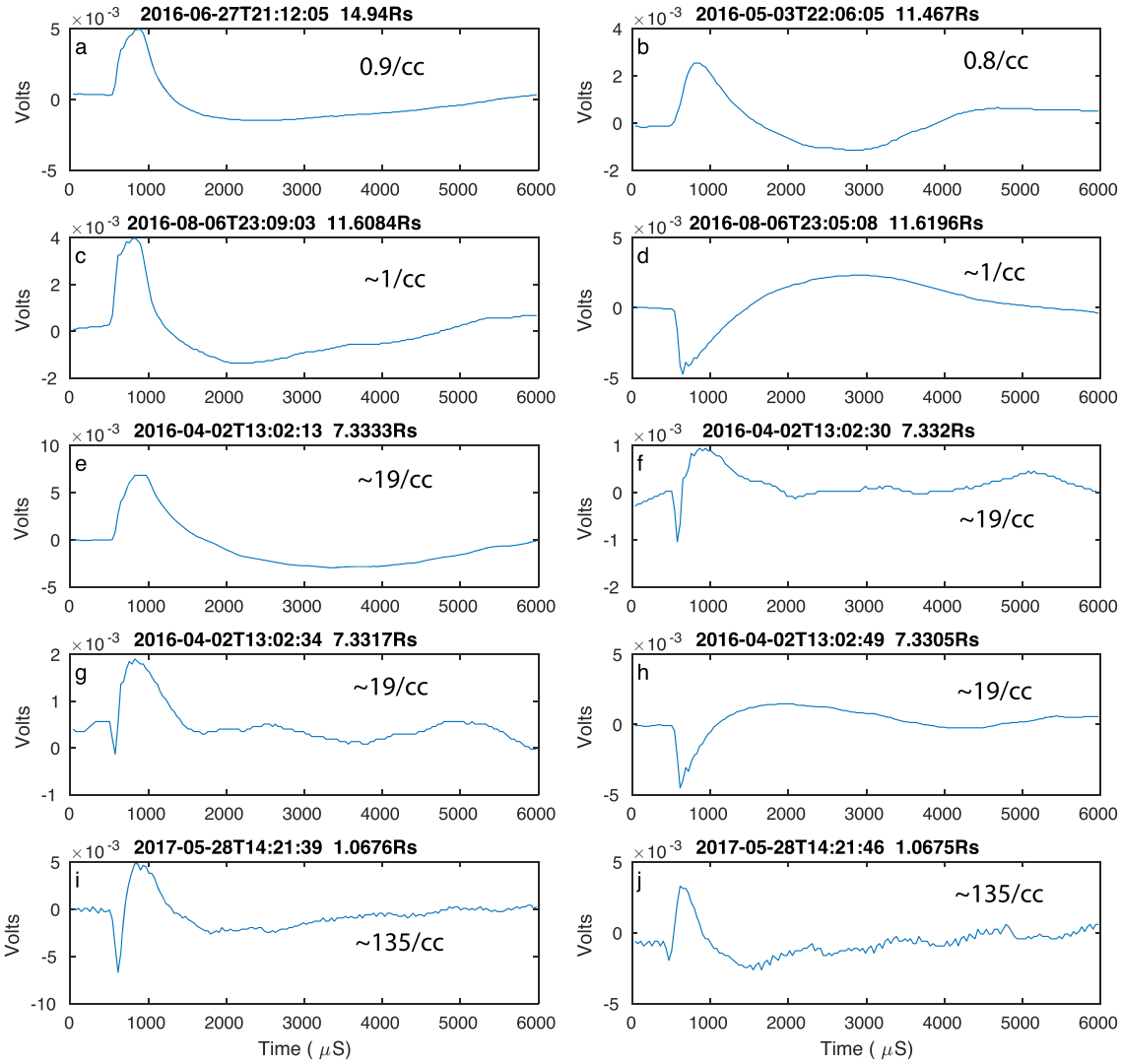

Figure 1. Panels (a–j) Example raw waveforms of dust impact signals captured by Cassini Radio and Plasma Wave Science (monopole mode) at different locations in Saturn's magnetosphere. The radial distances of observation are shown at the top of the panels. The electron densities are shown for each case.

Multiscale Mission waves instruments and reproduced in laboratory simulations and was proposed to be induced by image charging due to the faster escaping electrons in the impact plasma cloud (Collette et al., 2015; Nouzak et al., 2018).

4. Laboratory Simulations

The impact signal generation process can be simulated in the laboratory conditions, where the dust particles are accelerated to tens of kilometers per second before impacting a spacecraft model equipped with electric field antennas. The 3-MV Van de Graaff dust accelerator of Colorado IMPACT lab (Shu et al., 2012) was used to shoot micron-sized dust particles onto a 20:1 scaled-down Cassini model (Nouzak et al., 2018). The three antennas and the spacecraft body were connected to two preamplifiers and then digital oscilloscopes in order to measure the voltage signals on the dipole and monopole antennas at the same time. The antennas and the spacecraft body can also be biased to specific bias potentials with alkaline batteries. Tungsten targets were fixed on the spacecraft body and the antennas to enhance the impact charge yield and the impact signal. The model can be moved around in the vacuum chamber to control the target of impact (Nouzak et al., 2018). Precursor measurements were performed on identifying the basic signal generation mechanisms,

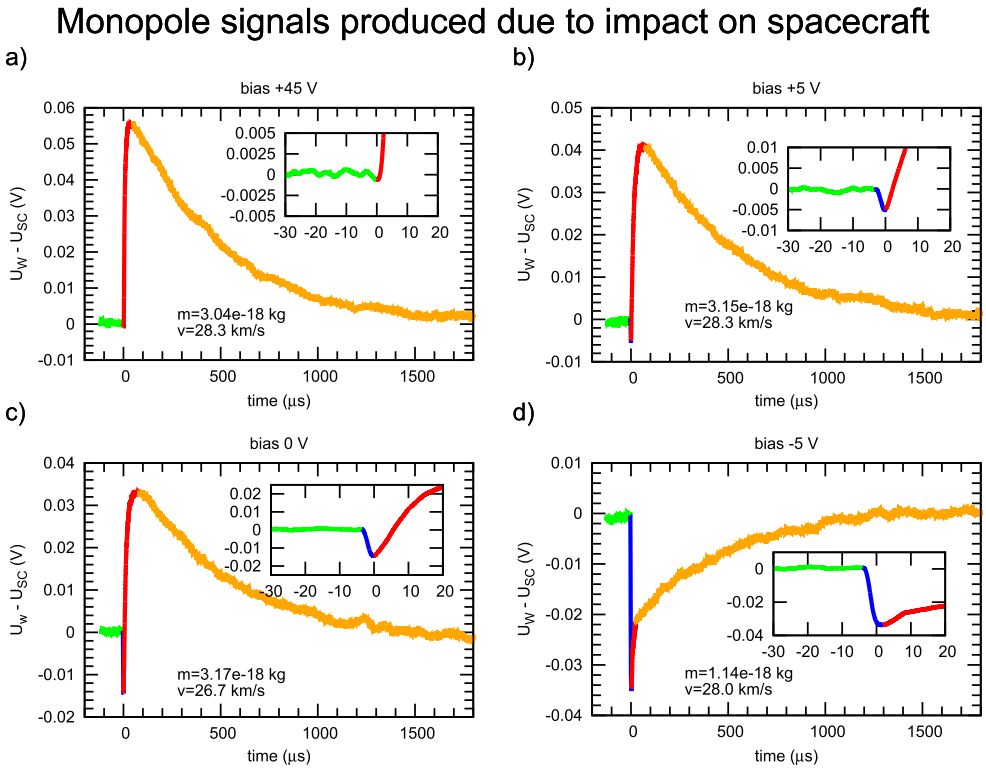

Figure 2. Panels (a–d) Monopole antenna signals triggered by iron dust impact on the spacecraft body (target on the High Gain Antenna). The signal shape changes with the bias potential (same bias for the spacecraft and antennas). The waveforms in the smaller boxes show the fine structure of the initial part of the signals. Color code indicate different parts of the signals (e.g., electron/ion escaping and relaxation).

measuring the charge yields from S/C relevant materials, or the rudimentary determination of the electron and ion temperatures in the impact plasma (Collette et al., 2014, 2015, 2016).

Figure S2 in the supporting information compares the dust impact signals measured under negative and positive bias potentials. As pointed out by Nouzak et al. (2018), the bias potential on the antenna determines the polarity of the impact signal. It is also noticed that the rise time for the positive bias potential case is significantly longer than the negative bias case (Ye, Kurth, Hospodarsky, Averkamp, Gurnett, Sternovsky, et al., 2016). The difference in polarity and in rise time scale indicates that the potential perturbation of the impact target is caused by the movement of different charge carriers (electron/ion), which are either attracted to or repelled from the impact site depending on the bias potential of the surface. Charged particles leaving the impact site constitute charging currents, which change the potential of the impact target (escaping ions/electrons can be deemed as negative/positive currents toward the spacecraft). In the negative bias potential case, the potential of the E_W antenna boom increases due to the escaping electrons, leading to a positive voltage pulse in the monopole channel (U_W-U_{SC}). The rise time is shorter than the positive bias case because electrons are ~40 times faster than ions (Lee et al., 2012, 2013; Fletcher & Close, 2017).

Figure 2 shows the monopole antenna signals triggered by iron dust impacts on the spacecraft body (the tungsten target was located on the High Gain Antenna). In the large positive bias case (Figure 2a), the signal is similar to the case shown in the right panel of Figure S2, except the polarity is reversed. The monopole channel measures the potential difference between the E_W antenna and the spacecraft body, so the polarity of the impact signal depends on the location of impact. In the small positive, zero, and negative bias potential cases (Figures 2b–2d), the signals consist of both a fast-decreasing part and a slow-rising part followed by a slow exponential decay (note the "kink" in the decay part of the signal in Figure 2d separating two different physical processes of different time scales). Two charging currents of different time scales are at work, changing the potential of the impact target. As the bias potential turns more negative, which would enhance the electron escape process and suppress the ion escape process, the fast part (pre-spike) increases in size, whereas the slow part shrinks. In Figure 2d, the slow part becomes smaller than the fast part due to the

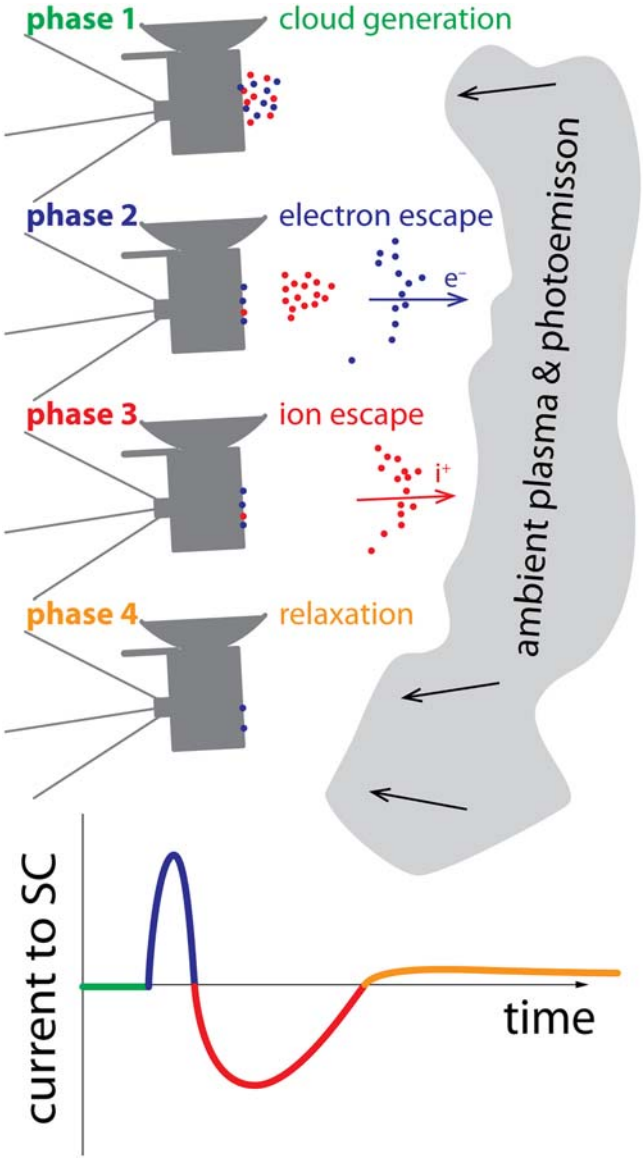

Figure 3. Evolution of the spacecraft charging current due to a dust impact (equilibrium spacecraft potential slightly positive due to low plasma density and stronger photoelectron emission): (Phase 1) Dust impact, impact cloud generation, recollection of charges, uncollected electrons, and ions are still near the spacecraft, the charging current remains close to zero. (Phase 2) Electron escape (energy of some electrons is large enough to leave the spacecraft): positive charging current, spacecraft potential increases. (Phase 3) Ion escape: follows the electron escape. More ions than electrons leave the spacecraft (slightly positive surface): negative charging current, spacecraft potential decreases to lower than equilibrium level. (Phase 4) Relaxation: the spacecraft potential returns to the equilibrium value due to ambient recharging, positive charging current due to photoelectron emissions, spacecraft potential increases back to equilibrium level.

enhancement of electron escape and the suppression of ion escape by the small negative bias potential. As a result, there is a kink that marks the end of the slow rising part and the decay part of the signal. The kink would disappear once the spacecraft bias potential becomes too negative (e.g., −25 V) for ions to escape. Fine time structures of the initial part of the signals (small box) show the different rates of spacecraft potential change due to electrons escaping (decreasing) and ions escaping (rising). The generation mechanism of a dust impact signal can be sketched in Figure 3, for a slightly positive spacecraft potential case (Figure 2b).

The decay time scales of the waveforms in Figure 2 are about the same (determined by the resistor-capacitor time of the electric circuit) for different bias potential settings. During the impact experiment, the Cassini model was placed in a vacuum chamber ($<10^{-5}$ torr), so the recharging current due to the background plasma is zero. The effect of background plasma on the impact signal shape can be tested in a chamber filled with plasma (future work) or numerically simulated.

5. Numerical Simulations

To simulate the Cassini spacecraft potential variation due to dust impacts, we used a simple numerical model described by Vaverka et al. (2017b) for spacecraft charging based on the Orbital Motion Limited theory (Mott-Smith & Langmuir, 1926), which includes photoemission and secondary electron emission. The currents due to dust impact (electron and ion escapes) are simulated as two independent currents by two Maxwellian functions with different time constants ($t_{esce} = 5.10^{-7}$ s and $t_{esci} = 5.10^{-6}$ s). The amount of charge generated is given by dust grain mass and impact velocity (Collette et al., 2014). We used $Q = 300$ pC in this study corresponding to the impact of a 1-μm grain at 25 km/s. We assume that half of the electrons and ions escape for uncharged spacecraft. The amount of the escaping particles depends on the spacecraft potential and their temperature. For example, the number of escaping electrons increases for negatively charged spacecraft and decreases for positively charged spacecraft.

Figure 4 shows the simulated variations of the spacecraft potential U_{SC} caused by dust impacts (top panel) and the deviation from the equilibrium potential dU_{SC} (bottom panel) for different ambient plasma conditions from 1 up to 1,000/cc. One per cc corresponds to >10 R_S at the Saturn equatorial plane (Persoon et al., 2013), and 1,000/cc corresponds to the Grand Finale orbits (Persoon et al., 2018; Wahlund et al., 2018). Plasma parameters chosen for Saturn's environment are shown in the legend boxes. The background plasma temperature is set to $T = 2$ eV and the impact plasma cloud temperature $T_c = 2$ eV, consistent with the values obtained by Cassini and laboratory measurement (Collette et al., 2016; Gustafsson & Wahlund, 2010; Schippers et al., 2013). The simulated impact signals show similar variation patterns as those detected in space (Figure 1) and laboratory (Figure 2) as the ambient plasma density and spacecraft potential change. The pre-spike and the kink in the decay part of the impact signals simulated in the laboratory can also be reproduced by this simple model.

The polarities of the signals are opposite to those shown in Figure 1 because the change in spacecraft potential (U_{SC} rather than U_W-U_{SC}) is plotted here. In the low negative spacecraft potential cases, the signal due to escaping ions can be identified as the fast "recovery" immediately after the positive voltage jump and prior to

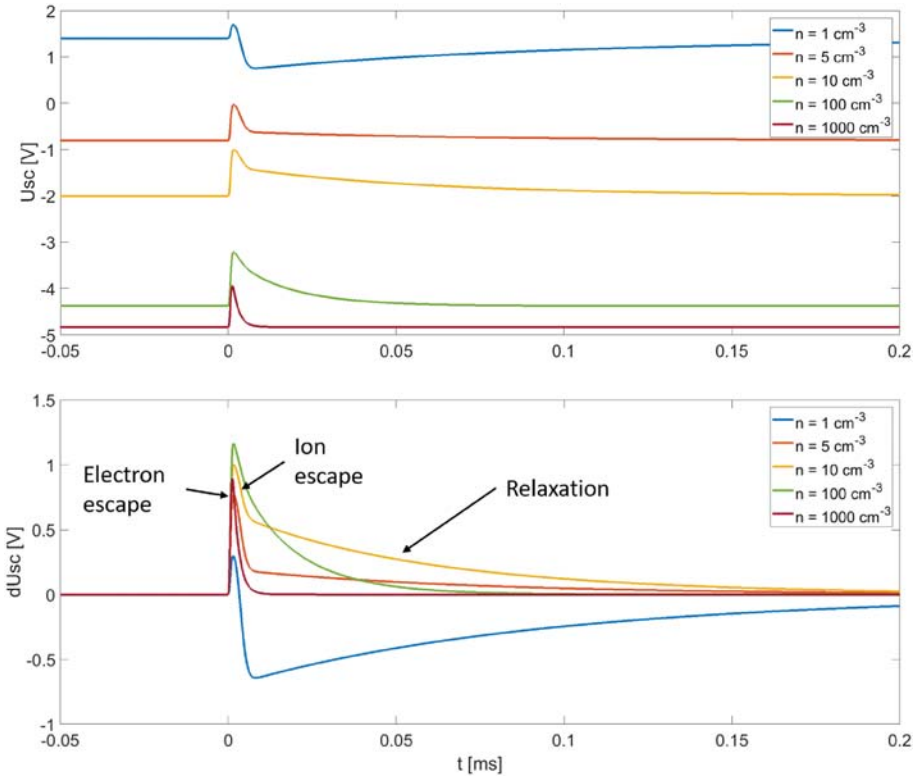

Figure 4. Potential variation of the Cassini spacecraft U_{SC} (top panel) and the deviation from the equilibrium potential dU_{SC} (bottom panel) due to interaction with the environment including a dust impact plasma cloud. The background plasma densities used are shown in the legend boxes.

the normal slow recovery due to the background plasma recharging. The transition from fast to slow recovery can be identified as the kink in the decay part of the simulated signals. Expanding ions of the impact-generated plasma constitute a negative charging current, decreasing the spacecraft potential at a slightly higher rate.

The decay (relaxation) time scale of the signals decreases with increasing background plasma density. It is shown that as the plasma density approaches 1,000/cc, the decay time scale is comparable to the rise time sale, and the size of the signal is also significantly reduced, reducing the sensitivity of electric field antennas to dust impacts in this situation (Vaverka et al., 2017b; Zaslavsky, 2015).

6. Discussion

Dust impact signals detected by the wave instruments are induced by the impact plasma cloud, which is generated by thermal ionization after the impactor and more target material are vaporized at the impact site. Collisions at the first stage of the plasma cloud expansion thermalize the plasma so that about half of the impact charges, whether electrons or ions, move toward the spacecraft and the other half move away. The thermalization (equal electron and ion temperature) makes electrons escape much faster than ions once the plasma cloud enters single particle motion regime. The resulting charge separation is crucial in causing the potential perturbation of the impact target (Meyer-Vernet et al., 1986; Oberc et al., 1990; Oberc, 1994; Pantellini, Landi, et al., 2012). It is possible to detect the changes in spacecraft potential only when electrons and ions move separately (e.g., electrons get collected and ions escape due to a positive spacecraft potential). The electrons and ions of an impact plasma cloud recollected or still in the vicinity of the spacecraft do not change its potential.

Early studies have attributed the generation of dust impact signals to the recollection of impact charges (Aubier et al., 1983; Gurnett et al., 1983; Meyer-Vernet, 1985). The charge recollection by the impact surface is a very fast process, which depends on Debye length of the ambient plasma, temperature of the impact

plasma, and the spacecraft potential. It is much shorter than the rise time scale observed in space and laboratory simulations. The impact signals are generated by removing charges from the impact surface rather than by charge recollection. Still, this does not completely rule out the results published in most previous studies based on charge collection model, since, in typical conditions, most of the electrons are collected and most ions repelled, as imagined by the authors of those previous studies.

The rise time is a function of the mass and velocity of the impactor and ambient plasma condition and determines the frequency range dust impact signals can be observed in wave instruments (Meyer-Vernet et al., 2017). Zaslavsky (2015) and Vaverka et al. (2017b) used a single parameter Δt (based on the rise times of impact signals observed in space) for the time scale of their charging currents when they simulated the change of spacecraft potential due to dust impacts. Some spaceborne wave instruments with low time resolution might not be able to resolve the faster rise time scale due to electron escapes. So the Δt observed in space, especially when spacecraft potential was negative, might just be the upper limit set by the sample time of the instrument (e.g., 36 μS for WBR 10-kHz mode). In laboratory simulations, longer rise times have been observed for impacts on the spacecraft body, which is a larger target than the antennas (Nouzak et al., 2018, fig. 5). The spacecraft body would have been a much more efficient charge recollector than the antennas. So the rise time of the impact signals is the time it takes for the escaping charges' influence on the target potential to diminish, which is longer for larger size targets. In space, the Debye length of ambient plasma/photoelectron determines how far the charges need to move away before they lose influence on the spacecraft potential. The impactor size and velocity play a role on the rise time scale, too, because they determine the energy (velocity) of the escaping charges and the amount of impact charges needed to be shielded from the spacecraft.

7. Conclusions

Laboratory simulations of dust impact signals detected in space helped us better understand the generation of such signals and how they can be picked up by electric field antennas. With ambient plasma parameters similar to those in different regions of Saturn's magnetosphere, numerical simulations of impact signals showed similar variation patterns as those measured in space and laboratory simulations. Depending on the spacecraft equilibrium potential, the electrons and ions of the impact plasma cloud are either attracted or repelled from the impact site, creating charge separations that alter the potential of the impact target. Electrons are significantly faster than ions, so the time scale for the charging current due to electron escaping is much shorter than that of ions. In cases of zero or slightly positive spacecraft potential, when part of the impact-generated electrons and ions can escape, a pre-spike (electron escaping signal) occurs before the main peak (ion escaping signal). The pre-spike disappears as the electron escaping process is suppressed by the increasing spacecraft potential. Similarly, the ion escaping process can also be suppressed by a slightly negative spacecraft potential, in which case the electron escaping signal is larger than the ion escaping signal, leading to a kink in the decay part of the signal (the initial part of the signal decay is actually due to the ions leaving the impact location). The spacecraft returns to its equilibrium potential when the charging currents due to the dust impact diminish and ambient plasma and photoelectron charging currents (small but persistent) regain dominance.

The pre-spikes and kinks in the lab-simulated dust impact signals provided important hints to understanding the generation of the dust impact signals detected in space. It requires high sampling rate like that used in the lab to reveal these features. For instruments with lower sampling rates, for example, MMS Fields Suite, these features would be smeared out and hard to detect (Vaverka et al., 2018). Numerical models showing the capability of reproducing these features could be used to predict impact signal shapes for other space missions in unfamiliar environment, for example, Parker Solar Probe or Solar Orbiter, although cautions are needed with respect to the validity of Orbital Motion Limited theory near perihelion (Ergun et al., 2010; Marchand et al., 2014).

Acknowledgments
This research was supported by NASA through Contract 1415150 with the Jet Propulsion Laboratory and NASA CDAP grant (14397000) "Understanding Dust Dynamics in Saturn's E-ring Using CDA/RPWS measurements, Modeling and Laboratory Experiments". The contributions of L. N., J. V., and J. P. were supported by Czech ministry of education youth and sport under Contract LTAUSA 17066. The paper also benefitted from discussions in the team "Physics of Dust Impacts: Detection of Cosmic Dust by Spacecraft and its Influence on the Plasma Environment" supported by the International Space Science Institute (ISSI) at Bern. The RPWS data from the Cassini spacecraft used in this study are available through the Planetary Data System (PDS; https://pds-ppi.igpp.ucla.edu/mission/Cassini-Huygens/CO/RPWS). The laboratory and simulation data are uploaded to ResearchGate repository with DOI: 10.13140/RG.2.2.23430.93769.

References

Aubier, M. G., Meyer-Vernet, N., & Pedersen, B. M. (1983). Shot noise from grain and particle impacts in Saturn's ring plane. *Geophysical Research Letters*, *10*(1), 5–8. https://doi.org/10.1029/GL010i001p00005

Braslau, D. (1970). Partitioning of energy in hypervelocity impact against loose sand targets. *Journal of Geophysical Research*, *75*(20), 3987–3999. https://doi.org/10.1029/JB075i020p03987

Close, S., Linscott, I., Lee, N., Johnson, T., Strauss, D., Goel, A., et al. (2013). Detection of electromagnetic pulses produced by hypervelocity micro particle impact plasmas. *Physics of Plasmas*, *20*(9), 092102.
Collette, A., Grün, E., Malaspina, D., & Sternovsky, Z. (2014). Micrometeoroid impact charge yield for common spacecraft materials. *Journal of Geophysical Research: Space Physics*, *119*, 6019–6026. https://doi.org/10.1002/2014JA020042
Collette, A., Malaspina, D. M., & Sternovsky, Z. (2016). Characteristic temperatures of hypervelocity dust impact plasmas. *Journal of Geophysical Research: Space Physics*, *121*, 8182–8187. https://doi.org/10.1002/2015JA022220
Collette, A., Meyer, G., Malaspina, D., & Sternovsky, Z. (2015). Laboratory investigation of antenna signals from dust impacts on spacecraft. *Journal of Geophysical Research: Space Physics*, *120*, 5298–5305. https://doi.org/10.1002/2015JA021198
Ergun, R. E., Malaspina, D. M., Bale, S. D., McFadden, J. P., Larson, D. E., Mozer, F. S., et al. (2010). Spacecraft charging and ion wake formation in the near-Sun environment. *Physics of Plasmas*, *17*(7), 072903.
Fletcher, A., Close, S., & Mathias, D. (2015). Simulating plasma production from hypervelocity impacts. *Physics of Plasmas*, *22*(9), 093504.
Fletcher, A. C., & Close, S. (2017). Particle-in-cell simulations of an RF emission mechanism associated with hypervelocity impact plasmas. *Physics of Plasmas*, *24*(5), 053102.
Grün, E. (1984). *Impact ionization from gold, aluminum and PCB-Z*, *ESA Special Publication* (Vol. 224, pp. 39–41). ESA Spec. Publ., ESA SP.
Gurnett, D. A., Grün, E., Gallagher, D., Kurth, W. S., & Scarf, F. L. (1983). Micron-sized particles detected near Saturn by the Voyager plasma wave instrument. *Icarus*, *53*(2), 236–254. https://doi.org/10.1016/0019-1035(83)90145-8
Gurnett, D. A., Kurth, W. S., Granroth, L. J., Allendorf, S. C., & Poynter, R. L. (1991). Micron-sized particles detected near Neptune by the Voyager 2 plasma wave instrument. *Journal of Geophysical Research*, *96*(S01), 19177. https://doi.org/10.1029/91JA01270
Gurnett, D. A., Kurth, W. S., Kirchner, D. L., Hospodarsky, G. B., Averkamp, T. F., Zarka, P., et al. (2004). The Cassini Radio and Plasma Wave Science investigation. *Space Science Reviews*, *114*, 395–463.
Gurnett, D. A., Kurth, W. S., Scarf, F. L., Burns, J. A., Cuzzi, J. N., & Grün, E. (1987). Micron-sized particle impacts detected near Uranus by the Voyager 2 plasma wave instrument. *Journal of Geophysical Research*, *92*(A13), 14959. https://doi.org/10.1029/JA092iA13p14959
Gustafsson, G., & Wahlund, J. E. (2010). Electron temperatures in Saturn's plasma disc. *Planetary and Space Science*, *58*(7-8), 1018–1025. https://doi.org/10.1016/j.pss.2010.03.007
Hew, Y. M., Goel, A., Close, S., & Lee, N. (2018). Hypervelocity impact flash and plasma on electrically biased spacecraft surfaces. *International Journal of Impact Engineering*, *121*, 1–11. https://doi.org/10.1016/j.ijimpeng.2018.05.008
Hsu, H. -W., Schmidt, J., Kempf, S., Postberg, F., Moragas-Klostermeyer, G., Seiß, M., et al. (2018). Cosmic Dust Analyzer onboard Cassini collects material from Saturn's main rings. *Science*, *362*(6410), eaat3185. https://doi.org/10.1126/science.aat3185
Kelley, M. C., Pancoast, S., Close, S., & Wang, Z. (2012). Analysis of electromagnetic and electrostatic effects of particle impacts on spacecraft. *Advances in Space Research*, *49*(6), 1029–1033. https://doi.org/10.1016/j.asr.2011.12.023
Kellogg, P. J., Goetz, K., & Monson, S. J. (2016). Dust impact signals on the wind spacecraft. *Journal of Geophysical Research: Space Physics*, *121*, 966–991. https://doi.org/10.1002/2015JA021124
Kellogg, P. J., Goetz, K., & Monson, S. J. (2018). Are STEREO single hits dust impacts? *Journal of Geophysical Research: Space Physics*, *123*, 7211–7219. https://doi.org/10.1029/2018JA025554
Kurth, W. S., Averkamp, T. F., Gurnett, D. A., & Wang, Z. (2006). Cassini RPWS observations of dust in Saturn's E ring. *Planetary and Space Science*, *54*(9-10), 988–998. https://doi.org/10.1016/j.pss.2006.05.011
Lee, N., Close, S., Goel, A., Lauben, D., Linscott, I., Johnson, T., et al. (2013). Theory and experiments characterizing hypervelocity impact plasmas on biased spacecraft materials. *Physics of Plasmas*, *20*(3), 032901.
Lee, N., Close, S., Lauben, D., Linscott, I., Goel, A., Johnson, T., et al. (2012). Measurements of freely-expanding plasma from hypervelocity impacts. *International Journal of Impact Engineering*, *44*, 40–49. https://doi.org/10.1016/j.ijimpeng.2012.01.002
Li, J., Song, W., & Ning, J. (2014). Theoretical and numerical predictions of hypervelocity impact-generated plasma. *Physics of Plasmas*, *21*(8), 082112.
Malaspina, D. M., Horányi, M., Zaslavsky, A., Goetz, K., Wilson, L. B. III, & Kersten, K. (2014). Interplanetary and interstellar dust observed by the Wind/WAVES electric field instrument. *Geophysical Research Letters*, *41*, 266–272. https://doi.org/10.1002/2013GL058786
Malaspina, D. M., O'Brien, L. E., Thayer, F., Sternovsky, Z., & Collette, A. (2015). Revisiting STEREO interplanetary and interstellar dust flux and mass estimates. *Journal of Geophysical Research: Space Physics*, *120*, 6085–6100. https://doi.org/10.1002/2015JA021352
Malaspina, D. M., & Wilson, L. B. III (2016). A database of interplanetary and interstellar dust detected by the Wind spacecraft. *Journal of Geophysical Research: Space Physics*, *121*, 9369–9377. https://doi.org/10.1002/2016JA023209
Marchand, R., Miyake, Y., Usui, H., Deca, J., Lapenta, G., Matéo-Vélez, J. C., et al. (2014). Cross-comparison of spacecraft-environment interaction model predictions applied to solar probe plus near perihelion. *Physics of Plasmas*, *21*(6), 062901.
McBride, N., & McDonnell, J. A. M. (1999). Meteoroid impacts on spacecraft: Sporadics, streams, and the 1999 Leonids. *Planetary and Space Science*, *47*(8-9), 1005–1013. https://doi.org/10.1016/S0032-0633(99)00023-9
Meyer-Vernet, N. (1985). Comet Giacobini-Zinner diagnosis from radio measurements. *Advances in Space Research*, *5*(12), 37–46. https://doi.org/10.1016/0273-1177(85)90065-1
Meyer-Vernet, N., Aubier, M. G., & Pedersen, B. M. (1986). Voyager 2 at Uranus: Grain impacts in the ring plane. *Geophysical Research Letters*, *13*(7), 617–620. https://doi.org/10.1029/GL013i007p00617
Meyer-Vernet, N., Lecacheux, A., Kaiser, M. L., & Gurnett, D. A. (2009). Detecting nanoparticles at the radio frequencies: Jovian dust stream impacts on Cassini/RPWS. *Geophysical Research Letters*, *36*, 3103. https://doi.org/10.1029/2008GL036752
Meyer-Vernet, N., Lecacheux, A., & Pedersen, B. M. (1996). Constraints on Saturn's E ring from the Voyager 1 radio astronomy instrument. *Icarus*, *123*(1), 113–128. https://doi.org/10.1006/icar.1996.0145
Meyer-Vernet, N., Moncuquet, M., Issautier, K., & Lecacheux, A. (2014). The importance of monopole antennas for dust observations: Why Wind/WAVES does not detect nanodust. *Geophysical Research Letters*, *41*, 2716–2720. https://doi.org/10.1002/2014GL059988
Meyer-Vernet, N., Moncuquet, M., Issautier, K., & Schippers, P. (2017). Frequency range of dust detection in space with radio and plasma wave receivers: Theory and application to interplanetary nanodust impacts on Cassini. *Journal of Geophysical Research: Space Physics*, *122*, 8–22. https://doi.org/10.1002/2016JA023081
Mitchell, D. G., Perry, M. E., Hamilton, D. C., Westlake, J. H., Kollmann, P., Smith, H. T., et al. (2018). D-ring dust falling into Saturn's equatorial upper atmosphere. *Science*, *362*(6410), eaat2236. https://doi.org/10.1126/science.aat2236
Mott-Smith, H. M., & Langmuir, I. (1926). The theory of collectors in gaseous discharges. *Physical Review*, *28*(4), 727.
Nouzak, L., Hsu, S., Malaspina, D., Thayer, F. M., Ye, S.-Y., Pavlu, J., et al. (2018). Laboratory modeling of dust impact detection by the Cassini spacecraft. *Planetary and Space Science*, *156*, 85–91. https://doi.org/10.1016/j.pss.2017.11.014
Oberc, P. (1994). Dust impacts detected by Voyager-2 at Saturn and Uranus: A post-Halley view. *Icarus*, *111*(1), 211–226. https://doi.org/10.1006/icar.1994.1141

Oberc, P. (1996). Electric antenna as a dust detector. *Advances in Space Research*, *17*(12), 105–110. https://doi.org/10.1016/0273-1177(95)00766-8

Oberc, P., Parzydło, W., & Vaisberg, O. L. (1990). Correlations between the Vega 2 plasma wave (APV-N) and dust (SP-1) observations at Comet Halley. *Icarus*, *86*(1), 314–326. https://doi.org/10.1016/0019-1035(90)90221-T

O'Shea, E., Sternovsky, Z., & Malaspina, D. M. (2017). Interpreting dust impact signals detected by the STEREO spacecraft. *Journal of Geophysical Research: Space Physics*, *122*, 11,864–11,873. https://doi.org/10.1002/2017JA024786

Pantellini, F., Landi, S., Zaslavsky, A., & Meyer-Vernet, N. (2012). On the unconstrained expansion of a spherical plasma cloud turning collisionless: Case of a cloud generated by a nanometre dust grain impact on an uncharged target in space. *Plasma Physics and Controlled Fusion*, *54*(4), 045005. https://doi.org/10.1088/0741-3335/54/4/045005

Pedersen, B. M., Meyer-Vernet, N., Aubier, M. G., & Zarka, P. (1991). Dust distribution around Neptune: Grain impacts near the ring plane measured by the Voyager planetary radio astronomy experiment. *Journal of Geophysical Research*, *96*(S01), 19,187–19,196. https://doi.org/10.1029/91JA01601

Persoon, A. M., Gurnett, D. A., Leisner, J. S., Kurth, W. S., Groene, J. B., & Faden, J. B. (2013). The plasma density distribution in the inner region of Saturn's magnetosphere. *Journal of Geophysical Research: Space Physics*, *118*, 2970–2974. https://doi.org/10.1002/jgra.50182

Persoon, A. M., Kurth, W. S., Gurnett, D. A., Groene, J. B., Sulaiman, A. H., Wahlund, J. E., et al. (2018). Electron density distributions in Saturn's ionosphere. *Geophysical Research Letters*, *46*, 3061–3068. https://doi.org/10.1029/2018GL078020

Pickett, J. S., Kurth, W. S., Gurnett, D. A., Huff, R. L., Faden, J. B., Averkamp, T. F., et al. (2015). Electrostatic solitary waves observed at Saturn by Cassini inside 10 Rs and near Enceladus. *Journal of Geophysical Research: Space Physics*, *120*, 6569–6580. https://doi.org/10.1002/2015JA021305

Ratcliff, P. R., Burchell, M. J., Cole, M. J., Murphy, T. W., & Alladfadi, F. (1997). Experimental measurements of hypervelocity impact plasma yield and energetics. *International Journal of Impact Engineering*, *20*(6-10), 663–674. https://doi.org/10.1016/S0734-743X(97)87453-2

Schippers, P., Meyer-Vernet, N., Lecacheux, A., Belheouane, S., Moncuquet, M., Kurth, W. S., et al. (2015). Nanodust detection between 1 and 5 AU using Cassini wave measurements. *The Astrophysical Journal*, *806*(1), 77. https://doi.org/10.1088/0004-637X/806/1/77

Schippers, P., Meyer-Vernet, N., Lecacheux, A., Kurth, W. S., Mitchell, D. G., & André, N. (2014). Nanodust detection near 1 AU from spectral analysis of Cassini/Radio and Plasma Wave Science data. *Geophysical Research Letters*, *41*, 5382–5388. https://doi.org/10.1002/2014GL060566

Schippers, P., Moncuquet, M., Meyer-Vernet, N., & Lecacheux, A. (2013). Core electron temperature and density in the innermost Saturn's magnetosphere from HF power spectra analysis on Cassini. *Journal of Geophysical Research: Space Physics*, *118*, 7170–7180. https://doi.org/10.1002/2013JA019199

Shu, A., Collette, A., Drake, K., Grün, E., Horányi, M., Kempf, S., et al. (2012). 3 MV hypervelocity dust accelerator at the Colorado Center for Lunar Dust and Atmospheric Studies. *Review of Scientific Instruments*, *83*(7), 075108.

Song, W., Lv, Y., Li, J., Wang, C., & Ning, J. (2016). Influence of impact conditions on plasma generation during hypervelocity impact by aluminum projectile. *Physics of Plasmas*, *23*(7), 073506.

Song, W., Lv, Y., Wang, C., & Li, J. (2015). Investigation on plasma generated during hypervelocity impact at different impact velocities and angles. *Physics of Plasmas*, *22*(12), 123519.

Tarantino, P., Goel, A., Corso, A., Lee, N., & Close, S. (2018). An electrostatic method to model the expansion of hypervelocity impact plasma on positively biased surfaces. *Physics of Plasmas*, *25*(9), 092103. https://doi.org/10.1063/1.5039656

Tsintikidis, D., Gurnett, D., Granroth, L. J., Allendorf, S. C., & Kurth, W. S. (1994). A revised analysis of micron-sized particles detected near Saturn by the Voyager 2 plasma wave instrument. *Journal of Geophysical Research*, *99*(A2), 2261–2270. https://doi.org/10.1029/93JA02906

Tsintikidis, D., Kurth, W. S., Gurnett, D. A., & Barbosa, D. D. (1995). Study of dust in the vicinity of Dione using the Voyager 1 plasma wave instrument. *Journal of Geophysical Research*, *100*(A2), 1811–1822. https://doi.org/10.1029/94JA02357

Tsurutani, B. T., Clay, D. R., Zhang, L. D., Dasgupta, B., Brinza, D., Henry, M., et al. (2004). Plasma clouds associated with Comet P/Borrelly dust impacts. *Icarus*, *167*(1), 89–99. https://doi.org/10.1016/j.icarus.2003.08.021

Vaverka, J., Nakamura, T., Kero, J., Mann, I., De Spiegeleer, A., Hamrin, M., et al. (2018). Comparison of dust impact and solitary wave signatures detected by Multiple Electric Field Antennas onboard the MMS spacecraft. *Journal of Geophysical Research: Space Physics*, *123*, 6119–6129. https://doi.org/10.1029/2018JA025380

Vaverka, J., Pellinen-Wannberg, A., Kero, J., Mann, I., De Spiegeleer, A., Hamrin, M., et al. (2017a). Detection of meteoroid hypervelocity impacts on the Cluster spacecraft: first results. *Journal of Geophysical Research: Space Physics*, *122*, 6485–6494. https://doi.org/10.1002/2016JA023755

Vaverka, J., Pellinen-Wannberg, A., Kero, J., Mann, I., De Spiegeleer, A., Hamrin, M., et al. (2017b). Potential of Earth orbiting spacecraft influenced by meteoroid hypervelocity impacts. *IEEE Transactions on Plasma Science*, *45*(8), 2048–2055. https://doi.org/10.1109/TPS.2017.2676984

Wahlund, J.-E., Morooka, M. W., Hadid, L. Z., Persoon, A. M., Farrell, W. M., Gurnett, D. A., et al. (2018). In situ measurements of Saturn's ionosphere show that it is dynamic and interacts with the rings. *Science*, eaao4134. https://doi.org/10.1126/science.aao4134

Wang, Z., Gurnett, D. A., Averkamp, T. F., Persoon, A. M., & Kurth, W. S. (2006). Characteristics of dust particles detected near Saturn's ring plane. *Planetary and Space Science*, *54*(9-10), 957–966. https://doi.org/10.1016/j.pss.2006.05.015

Ye, S.-Y., Gurnett, D. A., & Kurth, W. S. (2016). In-situ measurements of Saturn's dusty rings based on dust impact signals detected by Cassini RPWS. *Icarus*, *279*, 51–61. https://doi.org/10.1016/j.icarus.2016.05.006

Ye, S. -Y., Gurnett, D. A., Kurth, W. S., Averkamp, T. F., Kempf, S., Hsu, H. W., et al. (2014). Properties of dust particles near Saturn inferred from voltage pulses induced by dust impacts on Cassini spacecraft. *Journal of Geophysical Research: Space Physics*, *119*, 6294–6312. https://doi.org/10.1002/2014JA020024

Ye, S.-Y., Kurth, W. S., Hospodarsky, G. B., Averkamp, T. F., & Gurnett, D. A. (2016). Dust detection in space using the monopole and dipole electric field antennas. *Journal of Geophysical Research: Space Physics*, *121*, 11,964–11,972. https://doi.org/10.1002/2016JA023266

Ye, S.-Y., Kurth, W.S., Hospodarsky, G.B., Averkamp, T.F., Gurnett, D.A., Sternovsky, Z., et al. (2016). Dust impact signals detected by Cassini RPWS: Observations and laboratory experiments, American Geophysical Union, Fall Meeting, San Francisco.

Ye, S. -Y., Kurth, W. S., Hospodarsky, G. B., Persoon, A. M., Gurnett, D. A., Morooka, M., et al. (2018). Cassini RPWS dust observation near Janus and Epimetheus orbits. *Journal of Geophysical Research: Space Physics*, *123*, 4952–4960. https://doi.org/10.1029/2017JA025112

Ye, S.-Y., Kurth, W. S., Hospodarsky, G. B., Persoon, A. M., Sulaiman, A. H., Gurnett, D. A., et al. (2018). Dust observations by the Radio and Plasma Wave Science Instrument during Cassini's Grand Finale. *Geophysical Research Letters*, *45*, 10–101. https://doi.org/10.1029/2018GL078059

Zaslavsky, A. (2015). Floating potential perturbations due to micrometeoroid impacts: Theory and application to S/WAVES data. *Journal of Geophysical Research: Space Physics*, *120*, 855–867. https://doi.org/10.1002/2014JA020635

Zaslavsky, A., Meyer-Vernet, N., Mann, I., Czechowski, A., Issautier, K., Le Chat, G., et al. (2012). Interplanetary dust detection by radio antennas: Mass calibration and fluxes measured by STEREO/WAVES. *Journal of Geophysical Research*, *117*, A05102. https://doi.org/10.1029/2011JA017480